Magnetic Resonance in Medicine 60:405–413 (2008)

Sensitivity of Diffusion Weighted Steady State Free Precession to Anisotropic Diffusion

Jennifer A. McNab* and Karla L. Miller

Diffusion-weighted steady-state free precession (DW-SSFP) accumulates signal from multiple echoes over several TRs yielding a strong sensitivity to diffusion with short gradient durations and imaging times. Although the DW-SSFP signal is well characterized for isotropic, Gaussian diffusion, it is unclear how the DW-SSFP signal propagates in inhomogeneous media such as brain tissue. This article presents a more general analytical expression for the DW-SSFP signal which accommodates Gaussian and non-Gaussian spin displacement probability density functions. This new framework for calculating the DW-SSFP signal is used to investigate signal behavior for a single fiber, crossing fibers, and reflective barriers. DW-SSFP measurements in the corpus callosum of a fixed brain are shown to be in good agreement with theoretical predictions. Further measurements in fixed brain tissue also demonstrate that 3D DW-SSFP out-performs 3D diffusion weighted spin echo in both SNR and CNR efficiency providing a compelling example of its potential to be used for high resolution diffusion tensor imaging. Magn Reson Med 60:405–413, 2008.

Key words: diffusion; steady-state free precession; anisotropy

Diffusion weighted steady state free precession (DW-SSFP) (1–10) is a unique alternative to standard diffusion-weighted spin-echo echo planar imaging (DW-SE-EPI). When a single, unbalanced gradient is added to the balanced steady-state free precession (SSFP) pulse sequence (Fig. 1), diffusion effects accumulate over multiple repetition times (TRs) resulting in a strong sensitivity to diffusion with only modest gradient strengths and durations. The high signal-to-noise ratio (SNR) and contrast-to-noise ratio (CNR) efficiency of DW-SSFP (3) make it an ideal candidate for high spatial and angular resolution diffusion imaging.

The measured DW-SSFP signal is a weighted combination of spin echo (SE) and multiple stimulated echo (STE) pathways each with its own *b*-value (1,5). For isotropic diffusion, the DW-SSFP signal is well-characterized (1,5) and quantitative measurements of the diffusion coefficient are possible in homogeneous phantoms provided T_1, T_2, and proton density are known (9). What has not been investigated previously is the more complicated condition of anisotropic diffusion. It is unclear how the DW-SSFP signal behaves in an environment such as brain tissue, where natural barriers such as cell membranes and large molecules restrict the diffusion molecules along certain directions. Even for a single fiber population it is not obvious what form the DW-SSFP signal profile will take or how it differs from that of DW-SE.

In this article, we present an expression for the DW-SSFP signal in terms of an arbitrary spin displacement probability density function (pdf). This more general form of the DW-SSFP signal equation is used to investigate the non-Gaussian pdfs associated with restriction and crossing fibers in addition to a simple single fiber population. The analytically derived DW-SSFP signal profiles for single and crossing fiber populations are validated through simulations and measurements in the postmortem brain tissue. Measurements are made using a variant of fully 3D DW-SSFP which includes a segmented EPI readout to increase scan efficiency. The sensitivity of DW-SSFP to anisotropic diffusion is studied across a range of different tissue parameters and a comparison of the SNR and CNR efficiency of DW-SSFP with DW-SE is made in postmortem tissue.

THEORY

Signal Model for Diffusion Weighted Steady State Free Precession

As with other steady-state imaging methods, the DW-SSFP signal results from multiple echo pathways, which evolve over many repetition times (TRs) (11). An expression for the DW-SSFP signal was first presented by Kaiser et al. (1) in the context of spectroscopy using a constant diffusion gradient and later modified to include pulsed diffusion gradients by Wu and Buxton (5,7). The key feature that distinguishes the DW-SSFP signal from other types of diffusion weighted pulse sequences (e.g., DW-SE or DW-STE) is that the diffusion-dependent terms are not separable from the other imaging parameters: T_1, T_2, TR, and flip angle (α) (Appendix A). Additionally, the complicated interdependence of the diffusion terms and the nondiffusion terms make it difficult to build intuition for how this pulse sequence will behave for a given parameter choice and/or tissue type.

One approach that has been used in the past to study DW-SSFP signal formation is referred to as the two transverse period approximation (7). If one assumes that T_2/TR is sufficiently small (<0.67), such that no magnetization will survive in the transverse plane for more than two TRs, then a simplified partition analysis may be used (7). In this approximation, the signal is the summation of echoes which have spent no more than two TRs in the transverse plane (T), interspersed with some number of intervals (m and n) in the longitudinal plane (L) (i.e., $L_1 \ldots L_m$ T

Department of Clinical Neurology, Oxford Centre for Functional Magnetic Resonance Imaging of the Brain, University of Oxford, Oxford, United Kingdom

Grant sponsor: Charles Wolfson Charitable Trust

*Correspondence to: Jennifer A. McNab, Oxford Centre for Functional Magnetic Resonance Imaging of the Brain, John Radcliffe Hospital, Headington, Oxford, OX3 9DU, United Kingdom. E-mail: jmcnab@fmrib.ox.ac.uk

Received 12 July 2007; revised 18 February 2008; accepted 24 March 2008.
DOI 10.1002/mrm.21668
Published online in Wiley InterScience (www.interscience.wiley.com).

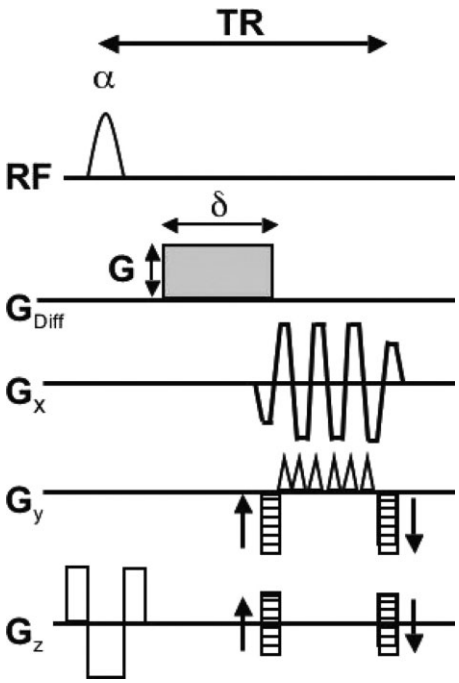

FIG. 1. Pulse sequence diagram for the variant of diffusion weighted steady state free precession (DW-SSFP) used in this study. DW-SSFP is characterized by low angle (α) RF pulses and short TRs. The current implementation uses a slab-selective excitation, slices encoded via phase-encoding and a segmented EPI read-out. With the exception of the single monopolar diffusion-sensitizing gradient (in gray), which can be applied along any direction, and has amplitude G and duration δ, all other gradients are fully balanced within each TR.

$L_1 \ldots . L_n$ T echo). The number of longitudinal periods between the two transverse periods (n) determines the mixing and diffusion time and will be referred to herein as the "echo number." For the special case of $n = 0$, a spin echo is formed. Although the two transverse period approximation is technically only valid within a specific range of T_2 and TR (7), it is often fairly accurate even outside of this parameter space since the echo pathways which propagate magnetization for more than two transverse periods contribute much less to the overall signal (7).

The DW-SSFP signal expression derived by Wu and Buxton (5,7) implicitly assumes Gaussian diffusion. It has long been recognized, however, that the Gaussian model of diffusion can be inappropriate when complex tissue structure is found within a single image voxel (12–16). Thus, it is useful to consider the DW-SSFP signal in terms of the reciprocal spatial wave vector ($\mathbf{q}$) and an arbitrary spin displacement pdf ($P(\mathbf{r}, \Delta)$) where for a square diffusion gradient pulse of amplitude $\mathbf{G}$ and duration δ:

$$\mathbf{q} = \frac{\gamma}{2\pi} \int_0^{\delta} \mathbf{G}(t)dt = \frac{\gamma}{2\pi}\mathbf{G}\delta \quad [1]$$

and $P(\mathbf{r}, \Delta)$ represents the probability of a molecule travelling a distance $\mathbf{r}$ in a time Δ. In the case of a conventional pulsed gradient spin-echo experiment, the signal attenuation ($E(\mathbf{q}, \Delta)$) is given by (17):

$$E(\mathbf{q}, \Delta) = \int P(\mathbf{r}, \Delta) exp(-i2\pi\mathbf{q} \cdot \mathbf{r})d\mathbf{r} \quad [2]$$

Buxton's simplified signal expression for DW-SSFP which uses the two transverse period approximation (7) can be adapted to accommodate any given spin displacement pdf if we avoid the assumption of Gaussian diffusion prior to summation of each of the individual echo paths. Assuming the narrow pulse approximation ($\delta \ll \Delta$) and following the physical arguments used in Buxton's approximate partition analysis (7), the signal for a given stimulated echo pathway contributing to the total DW-SSFP signal can be written as:

$$S_{\mathrm{STE}}(n, m) = -M_0(1 - E_1)E_1E_2^2 sin^3\alpha (E_1 cos\alpha)^m (E_1 cos\alpha)^{n-1} \times E(\mathbf{q}, \Delta = (n + 1) \times \mathrm{TR}) \quad [3]$$

where

m = the number of longitudinal periods preceding the first transverse period,
n = the number of longitudinal periods between the two transverse periods (i.e., echo number),
M_0 = equilibrium magnetization,
α = flip angle,
$E_1 = e^{-\frac{\mathrm{TR}}{T_1}}$,
$E_2 = e^{-\frac{\mathrm{TR}}{T_2}}$.

Equation [3] can be broken down into its component parts. $M_0(1 - E_1)$ accounts for the regrowth of longitudinal magnetization. E_1 represents longitudinal magnetization during the final longitudinal period. For each of the two transverse periods, transverse relaxation attenuates the signal by a factor E_2. When the magnetization transitions from the transverse plane to the longitudinal plane or vice versa, the signal is reduced by a factor of $sin\alpha$ and this occurs $3\times$ for a STE pathway.

For each of the m longitudinal periods that occur before the first transverse period, the signal is attenuated by a relaxation factor E_1 and reduced by a factor $cos\alpha$ by each RF pulse. The same signal reduction is taken into account for each of the n longitudinal periods between the two transverse periods (with the exception of the final longitudinal period which has already been accounted for). Lastly, $E(\mathbf{q}, \Delta = (n + 1) \times \mathrm{TR})$ accounts for diffusion effects. Since diffusion effects depend only on n and not m, Eq. [3] can be summed over m using:

$$\sum_{m=0}^{\infty} r^m = \frac{1}{1 - r}, |r| < 1 \quad [4]$$

to yield the signal for the stimulated echo pathway with echo number n:

$$S_{\mathrm{STE}}(n) = \frac{-M_0(1 - E_1)E_1E_2^2 sin^3\alpha}{1 - E_1 cos\alpha}(E_1 cos\alpha)^{n-1} \times E(\mathbf{q}, \Delta = (n + 1) \times \mathrm{TR}) \quad [5]$$

A spin echo pathway also contributes to the DW-SSFP signal and is represented by the special case of $n = 0$. The SE signal contribution has been derived previously by

Buxton (7) and is given by:

$$S_{SE} = \frac{-M_0(1-E_1)E_2^2 sin\alpha(1-cos\alpha)}{1-E_1 cos\alpha} E(\mathbf{q}, \Delta = \mathrm{TR}) \quad [6]$$

In the case of a SE pathway, there is only one transition from the longitudinal plane to the transverse plane and thus only one factor of $sin\alpha$. The RF pulse between the two transverse periods reduces the y-component of magnetization by a factor of $cos\alpha$ and thus the total signal is reduced by a factor of $(1 - cos\alpha)$.

Combining Eqs. [5] and [6] we have:

$$S(n) = K \times L(n) \times E(\mathbf{q}, \Delta = (n+1) \times \mathrm{TR}) \quad [7]$$

with

$$K = \frac{-M_0(1-E_1)E_1E_2^2 sin\alpha}{1-E_1 cos\alpha} \quad [8]$$

and

$$L(n) = \begin{cases} E_1^{-1}(1-cos\alpha), & n=0 \\ sin^2\alpha(E_1 cos\alpha)^{n-1}, & n>0 \end{cases} \quad [9]$$

The measured DW-SSFP signal is thus given by:

$$S_{\mathrm{DWSSFP}} = \sum_{n=0}^{\infty} K \times L(n) \times E(\mathbf{q}, \Delta = (n+1) \times \mathrm{TR}) \quad [10]$$

In practice, the contribution of higher echo numbers is very small and thus we have found the summation of $n = 0$ to $n = 5$ to be sufficient. In contrast to the elegant Fourier transform relationship which exists between **q** and the signal attenuation in a DW-SE experiment Eq. [2] (17), for DW-SSFP the signal attenuation is given by a summation of many Fourier transforms where each Fourier transform represents a different contributing echo pathway with a different diffusion time given by: $\Delta = (n+1) \times \mathrm{TR}$.

For the case of a single tensor, the multivariate, Gaussian spin displacement pdf is given by:

$$P(\mathbf{r}, \Delta) = \frac{1}{\sqrt{(4\pi\Delta)^3\ |\mathbf{D}|}} exp\left[\frac{-\mathbf{r}^T\mathbf{D}^{-1}\mathbf{r}}{4\Delta}\right] \quad [11]$$

where **D** is the diffusion tensor and **r** is a vector specifying the diffusion distance and orientation. The Fourier transform of Eq. [11] is given by:

$$E(\mathbf{q}, \Delta) = exp(-\Delta\mathbf{q}^T\mathbf{D}\mathbf{q}). \quad [12]$$

Although, Eq. [12] is not valid for non-Gaussian spin displacement pdfs, using the new formalism, the Fourier Transform of any spin displacement pdf may be substituted into Eq. [10] to calculate the expected DW-SSFP signal. This allows for the investigation of DW-SSFP signal behavior for non-Gaussian systems such as crossing fibers and reflective barriers. The pdfs and attenuation terms for crossing fibers and reflective barriers are given in Appendices B and C. It should be noted that substituting the Fourier transformation of a spin displacement pdf into Eq. [10] will only yield the correct signal prediction for a valid narrow pulse approximation (i.e., $\delta \ll \Delta$). Although this approximation can never be realized exactly in a real experiment, Eq. [10] still provides powerful insight into more complicated diffusive displacements.

Buxton's full analytical expression for the DW-SSFP signal (7) (Appendix A) that accounts for all echo pathways (including those with more than two transverse periods) cannot easily adopt the model-free framework of **q**-space imaging since it is derived from a Fourier expansion with boundary conditions that can only be solved with some assumption about how diffusion propagates over time. In this article, we use Buxton's full analytical expression [Eq. A.1] to model signal profiles for a single fiber population and we use the two transverse period approximation (as written in Eq. [10]) to model signal from crossing fibers and reflective barriers. In all three cases (i.e., a single fiber, crossing fibers, and reflective barriers), Eq. [7] is used to study the signal contributions of different echo pathways.

METHODS

DW-SSFP Signal Profiles for a Single Fiber Population

Analytical DW-SE and DW-SSFP signal profiles were simulated in two dimensions assuming a diffusion tensor with fractional anisotropy (FA) = 0.9, Trace = 1.1×10^{-3} mm^2/sec. The root mean square displacement of diffusing particles within a fiber is described by an ellipse. Plotting the apparent diffusion coefficient (ADC) in all directions results in a distinct peanut shape corresponding to

$$\mathrm{ADC}_i = \hat{\mathbf{u}}_i^T\mathbf{D}\hat{\mathbf{u}}_i \quad [13]$$

where ADC_i represents the diffusivity along the direction specified by the unit vector $\hat{\mathbf{u}}_i$ for a tensor **D**. Signal profiles were generated by substituting ADC_i for the diffusion coefficient (D) in the full DW-SSFP signal equation (Eq. [A.1]) and the DW-SE signal Eq. [18] given by:

$$S_{\mathrm{DWSE}} = S_{\mathrm{DWSE}}(b=0)exp(-bD) \quad [14]$$

The following parameters were used to generate the DW-SSFP signal profile: $\alpha = 30°$, $T_1/T_2/\mathrm{TR} = 700/50/45$ msec, diffusion gradient amplitude (G) = 40 mT/m, duration of diffusion gradient pulse (δ) = 12 msec. These parameters are representative of an in vivo acquisition (8). Likewise a DW-SE signal profile was generated using Eq. [14] with $b = 3000$ s/mm^2. These parameters were also used by substituting Eq. [12] into Eq. [7] to simulate individual DW-SSFP echo pathways with $n = 2$, 4, and 8. To study the effect of each parameter individually (using Eq. [A.1]), DW-SSFP parameters including: δ, α, TR, T_1, and T_2 were varied one at a time to study their effect on the resultant signal profile.

Monte Carlo methods were used to simulate the stochastic motion and magnetization evolution of individual protons. The 2D diffusion of 10,000 protons were simulated with $\Delta t = 50\ \mu s$ time steps for a total time period of 10 s. The resultant spin displacements were calculated for a single tensor with $\lambda_1/\lambda_2 = 1 \times 10^{-3}/1 \times 10^{-4}$ mm^2/sec. Diffusing spins were simulated with a series of random displacements (l_D) generated from a Gaussian distribution with mean $\langle l_\mathrm{D}\rangle = 0$ and standard deviation $\sigma l_\mathrm{D} = \sqrt{(2\lambda_1\Delta)}$ along its principal diffusion axis and $\sigma l_\mathrm{D} = \sqrt{(2\lambda_2\Delta)}$ along its secondary diffusion axis. The appropriate matrices governing RF pulse rotation, T_1/T_2 relaxation and diffusion gradient dephasing were applied to each of the protons for consecutive TRs using $\alpha = 30°$, $\mathrm{TR}/T_1/T_2 = 45/700/50$

msec, $G = 40$ mT/m, and δ = 8, 12, and 20 msec. Simulations were repeated for 30 diffusion directions in the plane of the tensor ($\Delta\theta = 6°$). The simulation commenced with all spins at (0,0) and total magnetization $[M_x, M_y, M_z] = [0, 0, 1]$. The diffusion gradient was assumed to be the only source of dephasing within each TR. At the end of the simulation, the DW-SSFP signal was calculated from the complex summation of all of the proton's individual magnetizations.

DW-SSFP Signal Profiles for Crossing Fibers

DW-SSFP signal profiles for two fibers oriented orthogonal to each other were simulated in 2D by substituting Eq. [A.3] into Eq. [10] and calculating the summation from $n = 0$ to $n = 5$. Using the same Monte Carlo methods described earlier for the single tensor the resultant spin displacements of two tensors were simulated to further verify the general form of the DW-SSFP signal equation (Eq. [10]). Each of the two tensors had $\lambda_1/\lambda_2 = 1 \times 10^{-3}/1 \times 10^{-4}$ mm^2/sec and they were oriented orthogonal to each other at 45° and 135° with an equal number of spins attributed to each tensor ($f = 0.5$).

DW-SSFP Signal for Reflective Barriers

The effect of restriction on the DW-SSFP signal was investigated using the one dimensional example of perfectly reflecting barriers separated by a distance a. The resultant DW-SSFP signal was calculated by the summation of Eq. [10] from $n = 0$ to $n = 5$ and the governing pdf given by Tanner and Stejskal (19) as listed in Appendix C. Parameters were: $\alpha = 30°$, TR/T_1/T_2 = 45/700/90 msec, $G = 40$ mT/m, and $\delta = 20$ msec. The diffusion coefficient was assumed to be 1×10^{-3} mm^2/sec.

Measurements in Fixed Brain Tissue

Imaging was performed at 3T using a 4-channel array of surface coils for signal reception. Data were acquired on a fixed macaque brain with the goals of assessing the SNR and CNR efficiency of DW-SSFP relative to DW-SE and validating the theoretical behavior of DW-SSFP for a single fiber population. A 9 year old male macaque (*Macaca mulatta*) brain was obtained from an ongoing study of anterior cingulate cortex lesions. All procedures were conducted under project and personal licenses issued by the British Home Office and in accordance with the British Animal Scientific Procedures Act (1986). The animal was anesthetized with sodium pentobarbitone and perfused with 90% saline and 10% formalin. The brain was then removed and placed in 10% sucrose formalin for 24 hours prior to imaging. During the experiment the fixed brain was immersed in a proton-free fluid called Fomblin LC/8 (Solvay Solexis Inc.) and tightly secured in a plastic container. Special care was taken to eliminate air-cavities and bubbles within the ventricles and on the surface of the brain. All scanning was performed at room temperature (approximately 23°C).

The aim of this experiment was to acquire data in the corpus callosum with very high angular resolution such that a clear visualization of the raw DW-SSFP signal profile could be made and compared with a theoretical prediction. It is prohibitively time-consuming to acquire diffusion measurements in 3D at sufficient angular resolution to obtain a clear picture of the signal profile. Therefore, we chose to measure the 2D projection of the 3D diffusive motion by obtaining measurements in a 2D plane that encompasses the principal diffusion direction of the corpus callosum.

DW-SSFP, DW-SE, T_1, and T_2 data were acquired in an axial slice at the level of the corpus callosum (CC) of the macaque brain. The orientation of the central axial slice was optimized by eye such that it ran parallel to the CC fibers. Analogous to the simulations, diffusion measurements included 29 isotropically sampled directions ($\Delta\theta = 6°$) in the 2D plane of the slices. For the DW-SE measurements, an optimized 3D segmented DW-SE-EPI pulse sequence was used with imaging parameters: $b = 3000$ sec/mm^2, TE/TR = 111/590 msec, $\alpha = 72°$, bandwidth (BW) = 801 Hz/pixel, 21 lines per segment and matrix size = 120 × 94 × 52. The 3D segmented DW-SE-EPI pulse sequence was optimized by obtaining a global estimate of T_1 prior to the experiment and determining the flip angle and TR that yielded the highest SNR efficiency. Similarly, a 3D segmented DW-SSFP-EPI pulse sequence (Fig. 1) was used with: TE/TR = 12/40 msec, $\alpha = 37°$, BW = 942 Hz/pixel, 25 lines per segment, matrix size = 120 × 166 × 52. Although, an SNR efficiency calculation could also be applied to the DW-SSFP, since this pulse sequence is primarily specific absorption ratio (SAR)-limited, for a given diffusion gradient duration and read-out time, the optimal parameter choice is usually found by selecting TE and TR to be as short as possible and the flip angle as high as possible without exceeding SAR limitations. This was the approach taken here. Despite the fact that SAR did not pose a risk to our fixed brain specimen, we did not have the permissions to disable the SAR monitors. DW-SE-EPI and DW-SSFP-EPI protocols had 720 μm × 720 μm in-plane resolution and 52 matched 1.4 mm slices. Both pulse sequences employed interleaved k-space segmentation. Diffusion weighting was always applied with the maximum available gradient strength of 40 mT/m. Three sets of DW-SSFP-EPI data were acquired, each with a different diffusion gradient duration: δ = 1.2, 4.4, and 8.8 msec. T_1 and T_2 were measured in the center two slices of the 3D diffusion acquisitions using 2D SE single-shot EPI (720 μm × 720 μm in-plane resolution, matrix = 120 × 104, BW = 772 Hz/pixel, 2.8 mm slice thickness) with TE = [43, 50, 57, 70, 90, 117, 155, 205] msec for T_2 measurement and a slice-selective inversion pulse applied for T_1 measurement using TI = [50, 200, 400, 650, 1, 000, 1, 500, 2, 200, 3, 000] ms.

Analysis

SNR measurements were made in the post-mortem macaque brain by measuring the mean DW-SE and DW-SSFP signal over all 2D sampled diffusion directions in the same ROI and the standard deviation of the noise in a background ROI of equal size. The noise correction factor for magnitude images was applied to these calculations (20). SNR measurements were normalized for the number of voxels in each acquisition. To compare the sensitivity of DW-SE and DW-SSFP pulse sequences to anisotropic diffusion the variance of the mean profile ($p^T p$) for a ROI was divided by the variance of the noise (σ^2) in each voxel belonging to the ROI to obtain an estimation efficiency ($\varepsilon = p^T p/\sigma^2$) (21) which is a predictor of CNR.

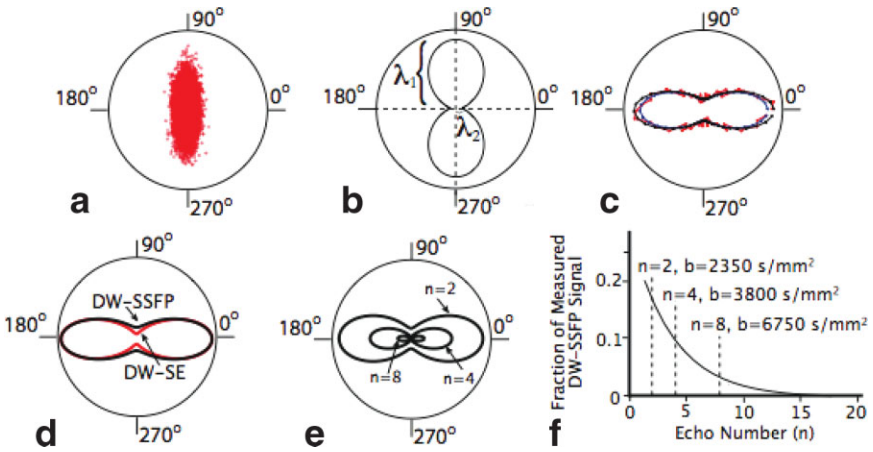

FIG. 2. (**a**) The final positions of 10,000 spins commencing at (0,0) and diffusing according to a tensor oriented at 90° with $\lambda_1/\lambda_2 = 1 \times 10^{-3}/1 \times 10^{-4}$. (**b**) The ADC profile for this tensor. (**c**) The resultant DW-SSFP signal profiles derived from the full analytical expression (Eq. A.1, black line), the two transverse period approximation (Eq. [10], blue line) and Monte Carlo simulations of the magnetization evolution of 10,000 spins (red line). (**d**) DW-SE (b = 3000 sec/mm^2, red line) and DW-SSFP (using Eq. [A.1] with $G/\delta = 40$ mT/m/12 msec, black line) signal profiles normalized along the minor diffusion axis and corresponding to the ADC profile shown in b). (**e**) Signal profiles for three individual echo pathways that contribute to the total measured DW-SSFP signal (largest to smallest: $n = 2$, 4, and 8). Note that these signal profiles have been scaled $\times 15$ for visualization purposes. (**f**) A plot of echo number (n) versus the relative contribution to the measured DW-SSFP signal. [Color figure can be viewed in the online issue, which is available at www.interscience.wiley.com.]

For the multi-echo and multi-TI SE data, voxel-wise T_1 and T_2 estimates were calculated using the governing signal expressions (22). A three parameter fit was performed for the multi-TI data to account for imperfect inversion pulses.

From an anatomical image, three regions of interest (ROIs) were selected in the splenium of the CC (Fig. 7a) such that each ROI would yield a distinct orientation of the principal diffusion axis within the 2D axial plane that the diffusion gradients were applied. Within these three ROIs, the voxel-wise T_1, T_2 estimates and diffusion signals were averaged. The mean diffusion signal measured at each orientation was plotted for DW-SE and DW-SSFP with all signals normalized to the largest measurement. Using Eq. [13], the DW-SE data was also used to calculate the ADC at each orientation. These ADC estimates along with T_1 and T_2 values for each ROI were substituted into the DW-SSFP signal equation (Eq. [A.1]) to facilitate a comparison between theoretical and empirical signal profiles.

RESULTS

Simulations

Figure 2a plots the final positions of 10,000 spins that commenced at the origin and diffused according to a single tensor oriented at 90° with $\lambda_1/\lambda_2 = 1 \times 10^{-3}/1 \times 10^{-4}$. Figure 2b shows the ADC profile corresponding to this tensor as given by Eq. [13]. In Figure 2c, the DW-SSFP signal profiles derived from the two transverse period approximation given by Eq. [10] (blue) and the full analytical expression given by Eq. [A.1] (black) are in good agreement. The two transverse period approximation slightly underestimates the signal along the secondary diffusion axis (Fig. 2c). This is expected since the criterion of $T_2 < 1.5$TR (7) is not satisfied. The DW-SSFP signal profile derived from the Monte Carlo simulations of individual spins (Fig. 2c, red line) is also in good agreement. Using 10,000 spins, Monte Carlo simulations ensures accuracy for signal values greater than $0.01 \times M_0$ (23) and thus the signal derived from these simulations becomes noisier along the principal diffusion axis (red line in Fig. 2c) where the signal drops slightly below this threshold.

Figure 2d compares the analytically derived signal profiles for DW-SSFP and DW-SE based on the single fiber population characterized in Figure 2a and b. The signal profile for DW-SSFP (derived using the full signal expression, Eq. [A.1]) has less narrowing at the principal diffusion axis compared to the signal profile for DW-SE. In our experience, regardless of the parameters chosen, the signal profiles for DW-SE or DW-SSFP never match. The reason for this difference in shape can be elucidated by studying the signal profiles for individual echo pathways that contribute to the DW-SSFP signal. By substituting Eq. [12] into Eq. [7], DW-SSFP profiles for echo pathways with $n = 2$, 4, and 8 and increasing b-values 2,350 sec/mm^2, 3,800 sec/mm^2, and 6,750 sec/mm^2 are shown in Figure 2e. While the signal profiles for larger echo numbers (i.e., longer diffusion time) have a much stronger sensitivity to diffusion anisotropy, they contribute less to the overall steady state signal (Fig. 2f). Thus, the weighted summation of all echo pathways results in a fundamentally different shape. Still, the DW-SSFP profiles demonstrate a clearly defined orientation of the principal diffusion axis.

Changes in the DW-SSFP signal profile with δ, α, TR, T_1, and T_2 can be seen in Figs. 3a–e. Increasing the diffusion gradient duration (Fig. 3a) increases the diffusion sensitivity with little effect on the intrinsic signal. Decreasing flip angle exhibits the opposite effect, it reduces the available signal with little effect on the shape of the profile (Fig. 3b). Increasing TR enhances diffusion weighting because it increases the diffusion time for all pathways (Fig. 3c) but also has the effect of attenuating the signal due to relaxation effects. For T_1, the DW-SSFP signal profile is relative

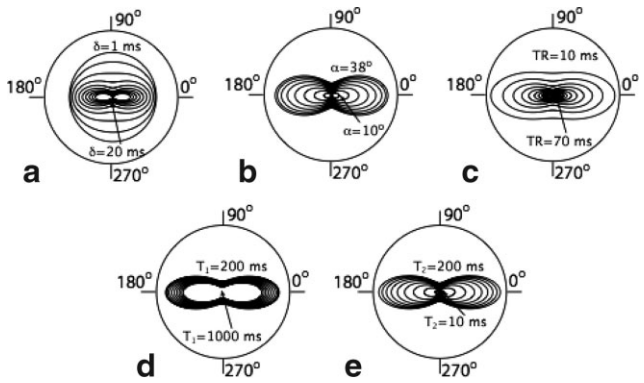

FIG. 3. Plots of DW-SSFP signal profiles with varying diffusion gradient duration (δ) (**a**), flip angle (α) (**b**), TR (**c**), T_1 (**d**), and T_2 (**e**). Default parameters used while varying each parameter individually were: G/δ = 40 mT/m/12 msec, $\alpha = 30°$, TR = 45 msec, $T_1 = 700$ msec, $T_2 = 50$ msec. DW-SSFP signal profiles will also modulate with G in a similar way that they do with δ. Note that for ease of visualization, a, d, and e have been scaled by $\times 3$ relative to b and c.

insensitive even over a wide range of relaxation times (Fig. 3d) and changing T_2 scales the DW-SSFP signal but does not greatly impact the sensitivity to anisotropic diffusion (Fig. 3e). Based on these simulations it appears that despite the complex interdependencies of all of these parameters, the diffusion gradient area is the most effective way of modulating the diffusion sensitivity of a DW-SSFP protocol. Aside from the the diffusion gradient, repetition time is the next most influential parameter on the sensitivity of the signal profiles to anisotropic diffusion with flip angle, T_1 and T_2 inducing little more than scaling factors.

Figure 4a shows the crossing fiber spin displacement profile for 10,000 spins, that began at (0,0) and diffused according to Eq. [A.2]. Figure 4b plots the resultant DW-SSFP signal profile for the spin displacement pdf modeled in Figure 4a. The analytical solution (Fig. 4b, blue line) is in good agreement with the Monte Carlo simulations (red line). In Figure 4c, the DW-SSFP signal profiles for five different echo pathways (Eq. [7], $n = 1$ to 5) are shown. The summation of these signals provides the analytical solution presented in Figure 4b. Each echo pathways that contributes to the measured DW-SSFP signal represents a snapshot of the spin displacement pdf at a well-defined diffusion time. Figures 4d–g show how the DW-SSFP signal profiles become less sensitive to the diffusion pattern as the duration of the diffusion gradient is reduced to 12 ms and 8 ms.

Figure 5 demonstrates that the DW-SSFP signal is expected to be sensitive to the effects of restriction. Signal curves as a function of **q** show well-defined zero crossings for specific restriction lengths (Fig. 5a). For the parameters used in Figure 5, it appears that DW-SSFP is sensitive to restriction on length-scales of 30 μm or less.

Measurements in Fixed Brain Tissue

Raw diffusion-weighted images in Fig. 6 demonstrate the high SNR efficiency of DW-SSFP compared with the optimized DW-SE acquisition. DW-SSFP images have 1.8× greater SNR than the matched DW-SE images

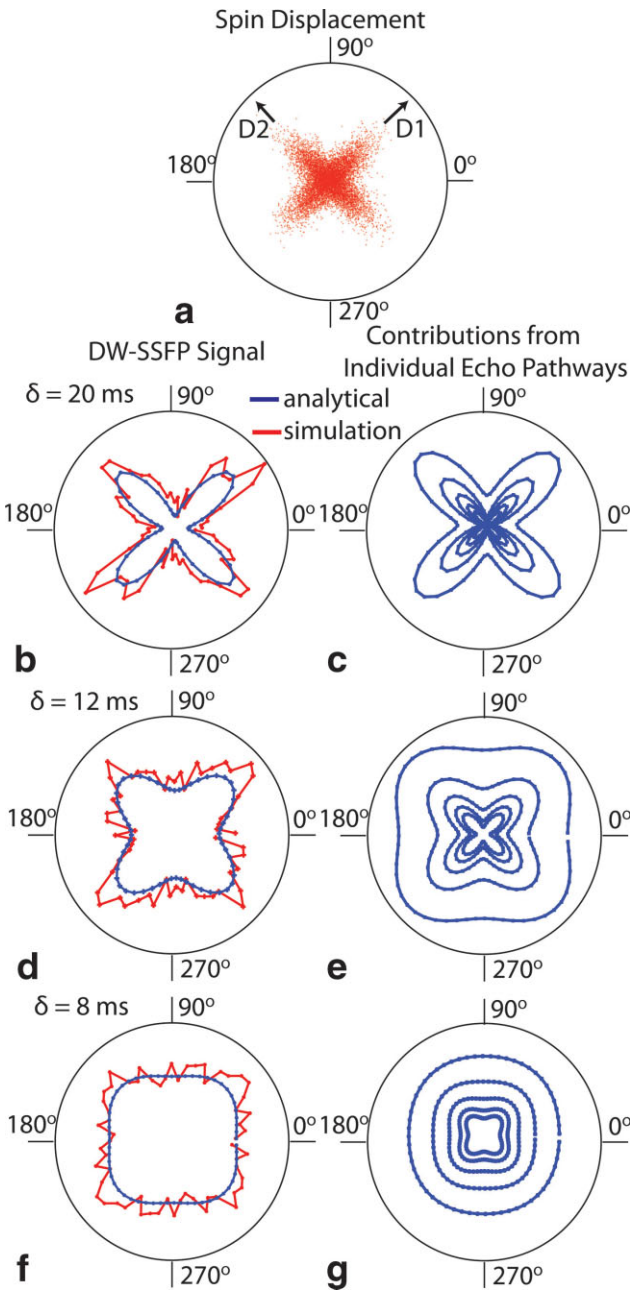

FIG. 4. (**a**) The spin displacement of 10,000 spins commencing at (0,0) and diffusing according to Eq. [A.2] for two equivalent tensors (D_1,D_2) oriented at 45° and 135°, each having $\lambda_1/\lambda_2 = 1 \times 10^{-3}/1 \times 10^{-4}$ mm^2/sec. Spins were divided equally between the two tensors (i.e. $f = 0.5$). (b) DW-SSFP signal profiles (using $\delta = 20$ msec) derived from the summation of Eq. [10] over $n = 0$ to $n = 5$ (blue) and the summation of individual protons magnetization evolutions (red). (**c**) Profiles of the DW-SSFP signal contributions from five different echo pathways. The echo pathway with the longest diffusion time ($n = 5$) is at the center and extending outward are echo pathways with decreasing diffusion times. (**d**–**g**) DW-SSFP profiles show the effect of decreasing the duration of the diffusion gradient to 12 msec and 8 msec. All signal profiles have been scaled uniformly and proportionately for visualization purposes. [Color figure can be viewed in the online issue, which is available at www.interscience.wiley.com.]

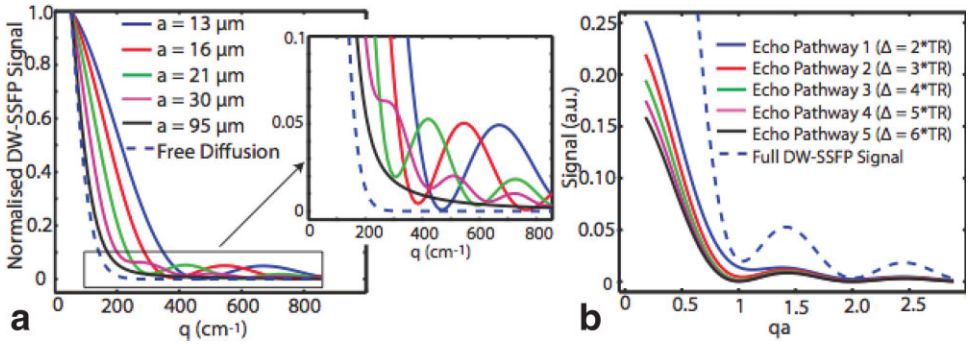

FIG. 5. Analytically derived DW-SSFP signal curves as a function of q for reflective barriers separated by varying distances *a*. (**b**) Signal contributions of individual echo pathways which each have their own diffusion time (Δ) and the full DW-SSFP signal (i.e., the weighted combination of signals from all five echo pathways) as a function of (qa) for $a = 21$ μm.

(SNR/voxel = 9 vs. SNR/voxel = 5) despite requiring only half the acquisition time (3 min vs. 6 min). In addition to the superior SNR efficiency, orientationally dependent diffusion contrast is clearly evident in the DW-SSFP images (Fig. 6). For example, both the left and right portions of the corpus callosum show strong attenuation when the diffusion encoding gradients are applied along the principal axis of the fiber (i.e., 48° and 135°), respectively. Likewise, the medial portion of the corpus callosum is not attenuated when the diffusion encoding gradients are applied perpendicular to the principal fiber axis (i.e., at 90°). A comparison of estimation efficiencies (ε) revealed values of 1.81 and 1.92 for DW-SE and DW-SSFP, respectively, indicating equivalent CNR. Given the reduced acquisition time, CNR efficiency favors DW-SSFP.

Figure 7 shows measured DW-SSFP signal profiles at three different diffusion weightings (δ = 1.2, 4.4 and 8.8 msec with G held constant at 40 mT/m) as well as measured DW-SE signal profiles ($b = 3,000$ sec/mm^2) from the three ROIs shown in Fig. 7a. As expected, the measured DW-SSFP signal profiles display increased sensitivity to anisotropic diffusion with increasing diffusion gradient duration (Fig. 7b–d). Although the DW-SSFP signal profiles with the highest diffusion weighting (δ/G = 8.8 msec/40 mT/m) show less narrowing along the principal fiber axis than for DW-SE with $b = 3,000$ sec/mm^2, a clear orientation is still evident. Agreement between empirical data and the predicted signal from measured T_1, T_2, and ADC_i (Fig. 7e) confirms that the DW-SSFP signal model is well-conditioned even under conditions of anisotropic diffusion. Note that by comparing the 2D analytical signal profile with the measured signal profile in the CC we have made the implicit assumption that the principal diffusion axis is oriented within the 2D sampling plane.

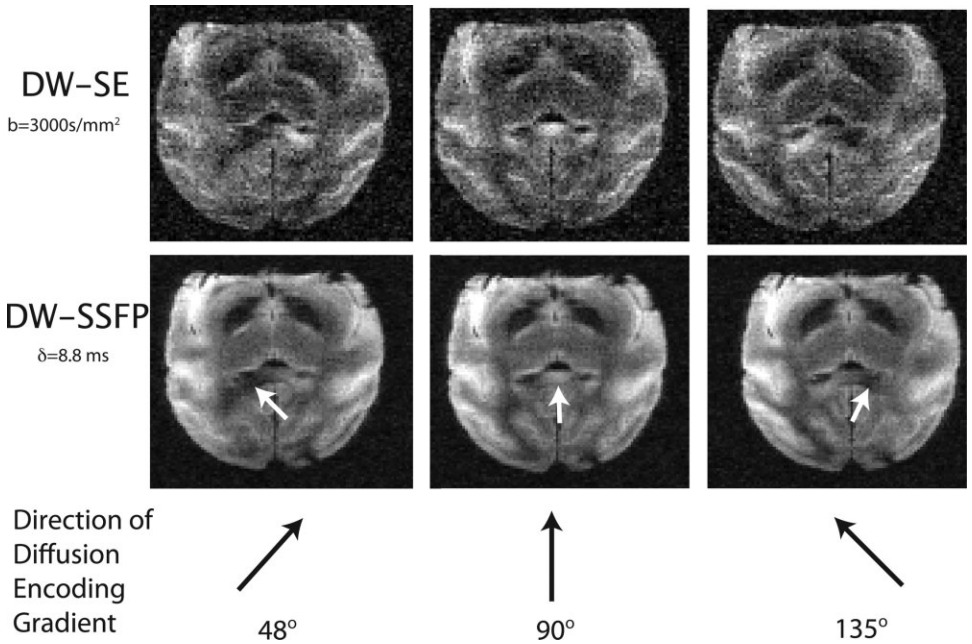

FIG. 6. Diffusion-weighted images (720 μm × 720 μm in-plane resolution, slice thickness = 1.4 mm) acquired in fixed macaque brain with diffusion encoding gradients applied at 48°, 90°, and 135° in-plane. Images in the top row were acquired using 3D segmented DW-SE-EPI (TE/TR = 111/590 msec, BW = 801 Hz/pixel, 21 lines per EPI segment, b = 3,000 sec/mm^2, acquisition time = 6 min, SNR/voxel = 5). Images in the bottom row were acquired using 3D segmented DW-SSFP-EPI (TE/TR = 12/40 ms, $\alpha = 37°$, 25 lines per EPI segment, BW = 942 Hz/pixel, diffusion gradient amplitude = 40 mT/m, diffusion gradient duration = 8.8 msec, acquisition time = 3 minutes, SNR/voxel = 9). White arrows highlight regions in the DW-SSFP images that show anisotropic contrast.

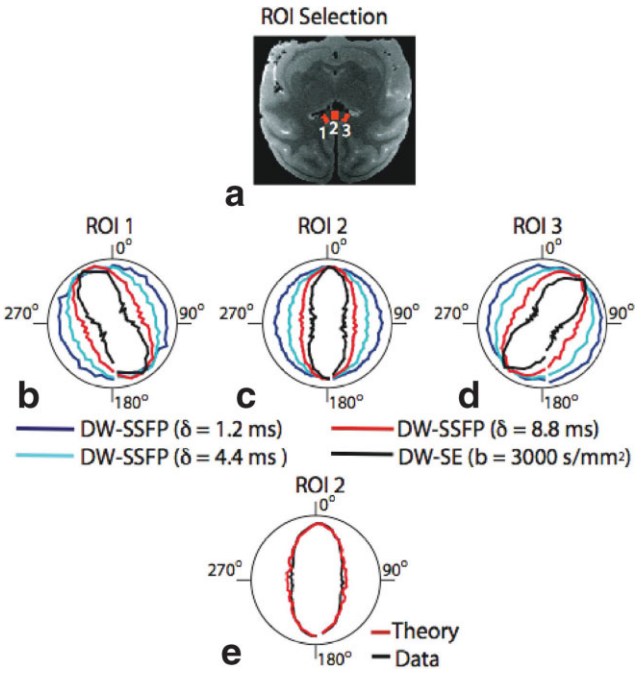

FIG. 7. (**a**) Three regions of interest (ROIs) in the splenium of the corpus callosum of a fixed macaque brain from which diffusion-weighted signal profiles were obtained (**b**–**d**). Signal profiles are shown for DW-SSFP at three different diffusion weightings, $\delta = 1.2$, 4.4, and 8.8 msec (G held constant at 40 mT/m) and for DW-SE ($b = 3000$ sec/mm^2). In (**e**), a theoretical signal profile (red) is generated by substituting measured T_1, T_2, and ADC values (from DW-SE measurements) into the DW-SSFP signal equation (Eq. [A.1]) and compared with the empirical signal profile (black) for ROI 2.

DISCUSSION

In this study, we have investigated DW-SSFP signal properties under conditions of anisotropic diffusion through both simulations and measurements in fixed brain tissue. DW-SSFP was found to be sensitive to anisotropic diffusion and able to delineate the principal diffusion axis of a single fiber population. An expression for the DW-SSFP signal in terms of an arbitrary pdf has been presented and DW-SSFP signal profiles for the case of crossing fibers have been studied through both analytical and Monte Carlo simulations.

DW-SSFP is sensitive to the process of diffusion in a way that DWSE is not. A single DW-SSFP measurement is intrinsically sensitive to how the diffusion process propagates over time whereas DWSE signal depends only on the final spin displacement. Our forward model for the DW-SSFP signal in terms of an arbitrary pdf, has been shown to be well conditioned and although there does not exist a simple Fourier transform relationship between **q**-space and the spin displacement pdf, simulation results for crossing fibers and reflective barriers indicate that it should be possible to extract relevant information about tissue microstructure from DW-SSFP data.

There are several possible approaches that could be taken to extract quantitative parameters from DW-SSFP measurements. A method for inverting the signal equation and solving for the diffusion coefficient using DW-SSFP has been presented previously by Deoni et al. (9). Deoni's method could be used to measure ADC in multiple orientations and the results of which could then be fit to a tensor. Alternatively, since we have shown Buxton's signal model (7) for DW-SSFP to be well-conditioned within brain tissue, nearly any method of non-linear fitting could be applied to multi-angular DW-SSFP data. Bayesian fitting methods, as used for probablistic tractography algorithms (24) is one such example. Spherical harmonic decomposition methods (25) are another possibility. One point of consideration, for any quantitative approach to DW-SSFP is that the DW-SSFP signal is dependent on flip angle and at 3T especially, B_1^+ inhomogeneities need to be considered.

From fixed brain tissue measurements, a 3D DW-SSFP pulse sequence with a segmented EPI readout was found to have nearly double the SNR/voxel in half the acquisition time compared to an analogous 3D DW-SE-EPI pulse sequence while retaining high diffusion contrast. Taking imaging times into account, DW-SSFP also has higher CNR efficiency. Thus, DW-SSFP is a promising option for high spatial and angular resolution diffusion imaging.

CONCLUSIONS

This study is the first to characterize DW-SSFP signal dynamics under conditions of anisotropic diffusion. Simulated DW-SSFP signal profiles presented here provide a basis for building intuition as to how one might optimize a DW-SSFP acquisition and analyze multi-angle DW-SSFP data. The demonstrated SNR and CNR efficiency of DW-SSFP provide a compelling example of the potential to improve upon current achievable voxel sizes using conventional DW-SE protocols.

ACKNOWLEDGMENTS

The authors would like to acknowledge helpful discussions had with Drs. Saad Jbabdi, Timothy E.J. Behrens, Matthew F.S. Rushworth, and Heidi Johansen-Berg. Thanks to Prof. Tipu Aziz and Dr. Ned Jenkinson for the ex vivo specimen and to Dr. Matthew Robson for the RF coil.

APPENDIX A

The equation for the full DW-SSFP signal (S) as presented by Buxton (7) is:

$$S = \frac{-M_0(1-E_1)E_2A_2^{-\frac{2}{3}}\left(F_1 - E_2A_1A_2^{\frac{2}{3}}\right)\sin\alpha}{r - F_1 s} \qquad [A.1]$$

where

M_0 = equilibrium magnetization,

α = flip angle,

$F_1 = K - \sqrt{K^2 - A_2^2}$,

$K = \frac{1-E_1A_1\cos\alpha - E_2^2A_1^2A_2^{-\frac{2}{3}}(E_1A_1-\cos\alpha)}{E_2A_1A_2^{-\frac{4}{3}}(1+\cos\alpha)(1-E_1A_1)}$,

$r = 1 - E_1\cos\alpha + E_2^2A_1A_2^{\frac{1}{3}}(\cos\alpha - E_1)$,

$s = E_2A_1A_2^{-\frac{4}{3}}(1 - E_1\cos\alpha) + E_2A_2^{-\frac{1}{3}}(\cos\alpha - 1)$,

$$A_1 = e^{-bD},$$
$$A_2 = e^{-\beta D},$$
$$b = (\gamma G\delta)^2 \mathrm{TR},$$
$$\beta = (\gamma G\delta)^2 \delta,$$
$$E_1 = e^{-\frac{\mathrm{TR}}{T_1}},$$
$$E_2 = e^{-\frac{\mathrm{TR}}{T_2}}.$$

G and δ represent the amplitude and duration of the diffusion gradient, respectively. TR represents the repetition time, T_1 and T_2 are the longitudinal and transverse relaxation times, and D represents the diffusion coefficient.

APPENDIX B

Although a single fiber population can be approximated by Gaussian diffusion, the summation of two identical tensors at different orientations (i.e., crossing fibers) is a non-Gaussian spin displacement pdf represented by:

$$P(\mathbf{r}, \Delta) = f \times \frac{1}{\sqrt{(4\pi\Delta)^3\ |\mathbf{D}_1|}} exp\left(\frac{-\mathbf{r}^T\mathbf{D}_1^{-1}\mathbf{r}}{4\Delta}\right) + (1-f) \times \frac{1}{\sqrt{(4\pi\Delta)^3\ |\mathbf{D}_2|}} exp\left(\frac{-\mathbf{r}^T\mathbf{D}_2^{-1}\mathbf{r}}{4\Delta}\right) \quad [A.2]$$

where f is the fraction of spins governed by the first tensor ($\mathbf{D}_1$) and $(1-f)$ is the fraction of spins governed by the the second tensor ($\mathbf{D}_2$). The Fourier transform of Eq. [A.2] with respect to $\mathbf{q}$ is equal to:

$$E(\mathbf{q}, \Delta) = f \times exp(-\Delta\mathbf{q}^T\mathbf{D}_1\mathbf{q}) + (1-f) \times exp(-\Delta\mathbf{q}^T\mathbf{D}_2\mathbf{q}) \quad [A.3]$$

APPENDIX C

The exact general solution for the the spin displacement pdf governing the one dimensional example of perfectly reflective barriers separated by a distance a was first obtained by Tanner and Stejskal (19) and is given by:

$$P(r, \Delta) = 1 + 2\sum_{k=1}^{\infty} exp\left(-\frac{k^2\pi^2 D\Delta}{a^2}\right) cos\left(\frac{k\pi r}{a}\right) \quad [A.4]$$

and its Fourier transform has been shown to be (19):

$$E(q, \Delta) = \frac{2(1 - cos(2\pi qa))}{(2\pi qa)^2} + 4(2\pi qa)^2 \sum_{k=1}^{\infty} exp\left(-\frac{k^2\pi^2 D\Delta}{a^2}\right) \times \frac{1 - (-1)^k cos(2\pi qa)}{((2\pi qa)^2 - (k\pi)^2)^2} \quad [A.5]$$

REFERENCES

1. Kaiser R, Bartholdi E, Ernst RR. Diffusion and field-gradient effects in NMR Fourier spectroscopy. J Chem Phys 1974;60:2966–2979.
2. Patz S, Hawkes RC. The application of steady-state free precession to the study of very slow fluid flow. Magn Reson Med 1986;3:140–145.
3. LeBihan D. Intravoxel incoherent motion imaging using steady-state free precession. Magn Reson Med 1988;7:346–351.
4. Merboldt KD, Bruhn H, Frahm J, Gyngell ML, Hanicke W, Deimling M. MRI of "diffusion" in the human brain: New results using a modified CE-FAST sequence. Magn Reson Med 1989;9:423–429.
5. Wu E, Buxton R. Effect of diffusion on the steady-state magnetization with pulsed field gradients. J Magn Reson 1990;90:243–253.
6. Carney C, Wong S, Patz S. Analytical solution and verification of diffusion effect in SSFP. Magn Reson Med 1991;19:240–246.
7. Buxton R. The diffusion sensitivity of fast steady-state free precession imaging. Magn Reson Med 1993;29:235–243.
8. Miller KL, Pauly JM. Nonlinear phase correction for navigated diffusion imaging. Magn Reson Med 2003;50:343–353.
9. Deoni S, Peters T, Rutt B. Quantitative diffusion imaging with steady-state free precession. Magn Reson Med 2004;51:428–433.
10. Miller KL, Hargreaves BA, Gold GE, Pauly JM. Steady-state diffusion-weighted imaging of in vivo knee cartilage. Magn Reson Med 2004;51:394–398.
11. Hennig J. Echoes-How to generate, recognize, use or avoid them in MR-imaging sequences. Concepts Magn Reson 1991;3:125–143.
12. Basser PJ, Mattiello J, Le Bihan D. MR diffusion tensor spectroscopy and imaging. Biophys J 1994;66:259–267.
13. Alexander AL, Hasan KM, Lazar M, Tsuruda JS, Parker DL. Analysis of partial volume effects in diffusion-tensor MRI. Magn Reson Med 2001;45:770–780.
14. Frank LR. Anisotropy in high angular resolution diffusion-weighted magnetic resonance imaging. Magn Reson Med 2001;45:935–939.
15. Ozarslan E, Mareci TH. Generalized diffusion tensor imaging and analytical relationships between diffusion tensor imaging and high angular resolution diffusion imaging. Magn Reson Med 2003;50:955–965.
16. Liu C, Bammer R, Moseley ME. Limitations of apparent diffusion coefficient-based models in characterizing non-Gaussian diffusion. Magn Reson Med 2005;54:419–428.
17. Callaghan PT. Principles of nuclear magnetic resonance microscopy. Oxford University Press; 1991.
18. Torrey HC. Bloch equations with diffusion terms. Phys Rev 1956;104:563–565.
19. Tanner JE, Stejskal EO. Restricted self-diffusion of protons in colloidal systems by the pulse-gradient, spin-echo method. J Chem Phys 1968;49:1768–1777.
20. Gudbjartsson H, Patz S. Simultaneous calculation of flow and diffusion sensitivity in steady-state. Magn Reson Med 1995;567–579.
21. Dale AM. Optimal experimental design for event-related fMRI. Human Brain Mapp 1999;8:109–114.
22. Haacke EM, Brown RW, Thompson MR, Venkatesan R. Magnetic resonance imaging: Physical principles and sequence design. Wiley, 1999.
23. Duh A, Mohoric A, Stepisnik J. Computer simulation of the spin-echo spatial distribution in the case of restricted self-diffusion. J Magn Reson 2001;148:257–266.
24. Behrens TEJ, Woolrich MW, Jenkinson M, Johansen-Berg H, Nunes RG, Clare S, Matthews PM, Brady JM, Smith SM. Characterization and propagation of uncertainty in diffusion-weighted MR imaging. Magn Reson Med 2003;50:1077–1088.
25. Tournier JD, Calamante F, Gadian DG, Connelly A. Direct estimation of the fiber orientation density function from diffusion-weighted MRI data using spherical deconvolution. Neuroimage 2004;23:1176–1185.